1. THE MOMENT-BASED LOW-ORDER EQUATIONS

The formulation of the LO equations is similar to a discontinuous FE method. Weighted integrals of the the equations are taken with functions that have local support as weight functions. The equations are written with element-wise moments of I and T as unknowns. Leaving the solution in this form allows for use of information form a previous HO solution to eliminate auxillary unknowns from the equations. This is different than a standard Galerkin FE method [**?**] where a functional form of the solution is directly assumed. The final equations will have a similar form to S_2 equations, but we have not used a collocation method in angle, which should limit ray effects [**?**] in higher spatial dimensions. The equations eliminate extra spatial unknowns in a manner similar to to a linear-discontinuous FE method [13]. We also explore the possibility of using the MC solution to modify the discretization of the LO solution in Sec. 1.3. MOVE

The remainder of this chapter is structured as follows: the general moments will be derived and then the angular and spatial closure are discussed REWRITE. For simplicity, the backward Euler time discretization is used throughout this section. Sec. **??** will use the HO solution and MC transport to consistently close the equations in time, improving time accuracy.

1.1 Forming the Space-Angle Moment Equations

1.1.1 LO Spatial mesh and Finite-Element Spatial Moments

The LO equations are formulated over a FE mesh. The domain for the i-th spatial element (or cell) has support $x \in [x_{i-1/2}, x_{i+1/2}]$ with width $h_i = x_{i+1/2} - x_{i-1/2}$ and cell center $x_i = x_{i-1/2} + h_i/2$. There is a total of N_c elements, spanning the spatial domain $0 \leq x \leq X$. For simplicity, this spatial mesh is fixed throughout the

simulation. Mesh adaptation is only applied in the HO solver.

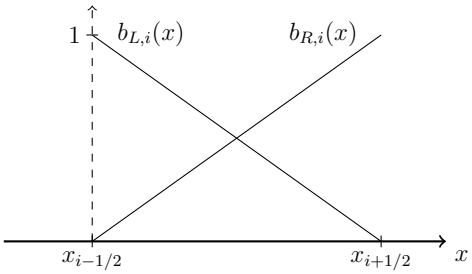

Figure 1.1: Illustration of linear finite element basis functions $b_{L,i}(x)$ and $b_{R,i}(x)$ for spatial element i.

The spatial moments are defined by integrals weighted with the standard linear finite element (FE) interpolatory basis functions. An illustration of the two linear FE basis functions for the i-th element is given in Fig. 1.1. The left basis function is defined as

$$b_{L,i}(x) = \begin{cases} \frac{x_{i+1/2}-x}{h_i} & x_{i-1/2} \leq x \leq x_{i+1/2} \\ 0 & \text{elsewhere} \end{cases}, \tag{1.1}$$

corresponding to the node $x_{i-1/2}$. The right basis function is

$$b_{R,i}(x) = \begin{cases} \frac{x-x_{i-1/2}}{h_i} & x_{i-1/2} \leq x \leq x_{i+1/2} \\ 0 & \text{elsewhere} \end{cases}, \tag{1.2}$$

corresponding to the node $x_{i+1/2}$. With these definitions, a local linear approximation to a function f can be formulated as $f(x) \simeq f_{L,i} b_{L,i}(x) + f_{R,i} b_{R,i}(x), \quad x \in [x_{i-1/2}, x_{i+1/2}]$.[1]

[1] In literature the FE functions are formally defined with support over two adjacent elements. However, in our notation our functions only have non-zero support in element i. This accommodates our later definition of moments and discontinuous unknowns.

The spatial moments are defined by integrals over the each element, using the two basis functions. We use $\langle\cdot\rangle$ to indicate integration over a spatial element. The spatial moments are

$$\langle\cdot\rangle_{L,i} = \frac{2}{h_i}\int_{x_{i-1/2}}^{x_{i+1/2}} b_{L,i}(x)(\cdot)\mathrm{d}x \tag{1.3}$$

and

$$\langle\cdot\rangle_{R,i} = \frac{2}{h_i}\int_{x_{i-1/2}}^{x_{i+1/2}} b_{R,i}(x)(\cdot)\mathrm{d}x. \tag{1.4}$$

where the factor of $2/h_i$ is a normalization constant. It is noted in this notation $\langle\phi\rangle_{L,i}$ and $\langle\phi\rangle_{R,i}$ represent spatial moments of the intensity over cell i, opposed to $\phi_{L,i}$ and $\phi_{R,i}$, which represent the interior value of the linear representation of $\phi(x)$ at $x_{i-1/2}$ and $x_{i+1/2}$ within the cell.

To simplify notation and discussion, we also define the slope and average moments over a spatial cell. The average scalar intensity is

$$\phi_i = \frac{1}{h_i}\int_{x_{i-1/2}}^{x_{i+1/2}} \phi(x)\mathrm{d}x \tag{1.5}$$

and

$$\phi_{x,i} = \frac{6}{h_i}\int_{x_{i-1/2}}^{x_{i+1/2}} \left(\frac{x-x_i}{h_i}\right)\phi(x)\mathrm{d}x. \tag{1.6}$$

The linear representation over a cell in terms of these moments is $\phi(x) = \phi_i + 2\phi_{x,i}(x - x_i)/h_i^2$, for $x \in (x_{i-1/2}, x_{i+1/2})$.

1.1.2 Definition of Angular Moments

To reduce the angular dimensionality, positive and negative half-range integrals of the angular intensity are taken. The angular integrals are denoted with a superscript as

$$(\cdot)^{\pm} = \pm\int_0^{\pm 1} (\cdot)\mathrm{d}\mu \tag{1.7}$$

The half-range integrals of I are defined as $\phi^+(x,t) = \int_0^1 I(x,\mu,t)\,\mathrm{d}\mu$ and $\phi^-(x,t) = 2\pi\int_{-1}^0 I(x,\mu,t)\,\mathrm{d}\mu$, respectively. Thus, in terms of half-range quantities, the mean intensity is $\phi = \phi^- + \phi^+$. It is noted that in this notation the flux is defined as $J = J^- + J^+$, which is not the standard definition for the half-range fluxes, e.g., in [10].

1.1.3 Space-Angle Moments of the Radiation Transport Equation

The LO radiation equations are formed by applying the space and angle moment operators to the transport equation and performing algebraic manipulation. We provide a detailed derivation of the L and $+$ radiation moment equation and state the final results for the other moment operators. First, the L moment operator is applied to the time-discretized transport equation, i.e., Eq. (**??**). Integration by parts on the streaming term yields

$$-\frac{2}{h_i}\mu_{i-1/2}I_{i-1/2}^{n+1} + \frac{2}{h_i^2}\int_{x_{i-1/2}}^{x_{i+1/2}} \mu I^{n+1}\mathrm{d}x + \left(\sigma_{t,i}^{n+1} + \frac{1}{c\Delta t}\right)\langle\phi\rangle_{L,i}^{n+1,+} - \frac{\sigma_{s,i}}{2}\langle\phi\rangle_{L,i}^{n+1} = \frac{1}{2}\langle\sigma_a^{n+1}acT^{n+1,4}\rangle_{L,i} + \frac{1}{c\Delta t}\langle\phi\rangle_{L,i}^{n,+}. \quad (1.8)$$

Here, the cross sections have been assumed constant over a cell. The mean intensity in the scattering term is expanded in terms of half-range unknowns. The integral can be rewritten in terms of L and R moments by noting that $b_{L,i}(x)+b_{R,i}(x) = 2/h_i$. These substitutions are made and the resulting equation is multiplied by h_i to produce

$$-2\mu_{i-1/2}I_{i-1/2}^{n+1} + \langle\mu I^{n+1}\rangle_{L,i} + \langle\mu I^{n+1}\rangle_{R,i} + \left(\sigma_{t,i}^{n+1} + \frac{1}{c\Delta t}\right)h_i\langle\phi\rangle_{L,i}^{n+1,+} - \frac{\sigma_{s,i}h_i}{2}\left(\langle\phi\rangle_{L,i}^{n+1,+} + \langle\phi\rangle_{L,i}^{n+1,-}\right) = \frac{h_i}{2}\langle\sigma_a^{n+1}acT^{n+1,4}\rangle_{L,i} + \frac{h_i}{c\Delta t}\langle\phi\rangle_{L,i}^{n,+}. \quad (1.9)$$

The resulting equation is integrated over the positive half range:

$$-2\left(\mu_{i-1/2}I_{i-1/2}^{n+1}\right)^{+}+\langle\mu I^{n+1}\rangle_{L,i}^{+}+\langle\mu I^{n+1}\rangle_{R,i}^{+}+\left(\sigma_{t,i}^{n+1}+\frac{1}{c\Delta t}\right)h_i\langle\phi\rangle_{L,i}^{n+1,+}$$
$$-\frac{\sigma_{s,i}h_i}{2}\left(\langle\phi\rangle_{L,i}^{n+1,+}+\langle\phi\rangle_{L,i}^{n+1,-}\right)=\frac{h_i}{2}\langle\sigma_a^{n+1}acT^{n+1,4}\rangle_{L,i}+\frac{h_i}{c\Delta t}\langle\phi\rangle_{L,i}^{n,+}. \quad (1.10)$$

1.1.4 The Angular Consistency Terms

Now, algebraic manipulations are performed on the streaming terms to produce face and volume-averaged values of μ, weighted by the intensity. Each term in the streaming term is multiplied by a factor of unity, with the desired unknown appropriate to each term in the numerator and denominator. Temporarily dropping the time index for clarity, the manipulations applied to the streaming term are as follows:

$$\left\langle\mu\frac{\partial I}{\partial x}\right\rangle_L^{+}=-\frac{2}{h_i}\left(\mu I_{i-1/2}\right)^{+}+\frac{1}{h_i}\left[\langle\mu I\rangle_{L,i}^{+}+\langle\mu I\rangle_{R,i}^{+}\right] \quad (1.11)$$

$$=-\frac{2}{h_i}\left(\mu I_{i-1/2}\right)^{+}\frac{(I_{i-1/2})^{+}}{(I_{i-1/2})^{+}}+\frac{1}{h_i}\left[\langle\mu I\rangle_{L,i}^{+}\frac{\langle I\rangle_{L,i}^{+}}{\langle I\rangle_{L,i}^{+}}+\langle\mu I\rangle_{R,i}^{+}\frac{\langle I\rangle_{R,i}^{+}}{\langle I\rangle_{R,i}^{+}}\right] \quad (1.12)$$

$$=-\frac{2}{h_i}\left\{\frac{(\mu I)_{i-1/2}^{+}}{\phi_{i-1/2}^{+}}\right\}\phi_{i-1/2}^{+}+\frac{1}{h_i}\left[\left\{\frac{\langle\mu I\rangle_{L,i}^{+}}{\langle\phi\rangle_{L,i}^{+}}\right\}\langle\phi\rangle_{L,i}^{+}+\left\{\frac{\langle\mu I\rangle_{R,i}^{+}}{\langle\phi\rangle_{R,i}^{+}}\right\}\langle\phi\rangle_{R,i}^{+}\right] \quad (1.13)$$

The ratios in braces are what we will formally define as *angular consistency terms*. These nonlinear functionals are approximated by the HO solver. The angular consistency term for the L and $+$ moments is defined as

$$\{\mu\}_{L,i}^{n+1,+}\equiv\frac{\langle\mu I^{n+1}\rangle_{L,i}^{+}}{\langle I^{n+1}\rangle_{L,i}^{+}}=\frac{\frac{2}{h_i}\int_0^1\int_{x_{i-1/2}}^{x_{i+1/2}}\mu\, b_{L,i}(x)I^{n+1}(x,\mu)\mathrm{d}x\mathrm{d}\mu}{\frac{2}{h_i}\int_0^1\int_{x_{i-1/2}}^{x_{i+1/2}}b_{L,i}(x)I^{n+1}(x,\mu)\mathrm{d}x\mathrm{d}\mu}. \quad (1.14)$$

The consistency terms on the face represent averaging at a point, with a similar definition as

$$\mu^+_{i+1/2} \equiv \frac{\left(\mu I_{i+1/2}\right)^+}{\phi^+_{i+1/2}} = \frac{\int_0^1 \mu I(x_{i+1/2},\mu)\mathrm{d}\mu}{\int_0^1 I(x_{i+1/2},\mu)\mathrm{d}\mu} \,. \tag{1.15}$$

There are analogous definitions for the R and $-$ moments. The moment of the streaming term for the L and $+$ operators becomes

$$\left\langle \mu\frac{\partial I}{\partial x}\right\rangle^+_L = -\frac{2}{h_i}\mu^+_{i-1/2}I^+_{i-1/2} + \frac{1}{h_i}\left[\{\mu\}^+_{L,i}\langle\phi\rangle^+_{L,i} + \{\mu\}^+_{R,i}\langle\phi\rangle^+_{R,i}\right] \tag{1.16}$$

It is noted that this expression does not contain a cross section in the denomainator, such as in the variable Eddington factor approach [**?**], thus this method will be stable in a void.

1.1.5 The Exact Radiation Moment Equations

A final expression for the moment equation resulting from application of the L moment and positive half-range integral is obtained by substituting the result of Eq. (1.16) into Eq. (1.10):

$$\begin{aligned} -2\mu^{n+1,+}_{i-1/2}\phi^{n+1,+}_{i-1/2} + \{\mu\}^{n+1,+}_{L,i}\langle\phi\rangle^{n+1,+}_{L,i} + \{\mu\}^{n+1,+}_{R,i}\langle\phi\rangle^{n+1,+}_{R,i} + \left(\sigma^{n+1}_{t,i} + \frac{1}{c\Delta t}\right)h_i\langle\phi\rangle^{n+1,+}_{L,i} \\ - \frac{\sigma_{s,i}h_i}{2}\left(\langle\phi\rangle^{n+1,+}_{L,i} + \langle\phi\rangle^{n+1,-}_{L,i}\right) = \frac{h_i}{2}\langle\sigma^{n+1}_a acT^{n+1,4}\rangle_{L,i} + \frac{h_i}{c\Delta t}\langle\phi\rangle^{n,+}_{L,i}, \end{aligned} \tag{1.17}$$

Similar derivations can be used to derive the other radiation moment equations. Pairwise application of the L and R basis moments with the $+$ and $-$ half-range integrals to Eq. (**??**) ultimately yields four moment equations per cell. The equation

for the R and $+$ moment is

$$2\mu^{n+1,+}_{i+1/2}\phi^{n+1,+}_{i+1/2} - \{\mu\}^{n+1,+}_{L,i}\langle\phi\rangle^{n+1,+}_{L,i} - \{\mu\}^{n+1,+}_{R,i}\langle\phi\rangle^{n+1,+}_{R,i} + \left(\sigma^{n+1}_{t,i} + \frac{1}{c\Delta t}\right)h_i\langle\phi\rangle^{n+1,+}_{R,i} - \frac{\sigma_{s,i}h_i}{2}\left(\langle\phi\rangle^{n+1,+}_{R,i} + \langle\phi\rangle^{n+1,-}_{R,i}\right) = \frac{h_i}{2}\langle\sigma^{n+1}_a acT^{n+1,4}\rangle_{R,i} + \frac{h_i}{c\Delta t}\langle\phi\rangle^{n,+}_{R,i}, \quad (1.18)$$

The equations for the negative half-range moment are identical to the above with the negative half-range superscripts replacing the positive. Explicitly,

$$-2\mu^{n+1,-}_{i-1/2}\phi^{n+1,-}_{i-1/2} + \{\mu\}^{n+1,-}_{L,i}\langle\phi\rangle^{n+1,-}_{L,i} + \{\mu\}^{n+1,-}_{R,i}\langle\phi\rangle^{n+1,-}_{R,i} + \left(\sigma^{n+1}_{t,i} + \frac{1}{c\Delta t}\right)h_i\langle\phi\rangle^{n+1,-}_{L,i} - \frac{\sigma_{s,i}h_i}{2}\left(\langle\phi\rangle^{n+1,+}_{L,i} + \langle\phi\rangle^{n+1,-}_{L,i}\right) = \frac{h_i}{2}\langle\sigma^{n+1}_a acT^{n+1,4}\rangle_{L,i} + \frac{h_i}{c\Delta t}\langle\phi\rangle^{n,-}_{L,i} \quad (1.19)$$

and

$$2\mu^{n+1,-}_{i+1/2}\phi^{n+1,-}_{i+1/2} - \{\mu\}^{n+1,-}_{L,i}\langle\phi\rangle^{n+1,-}_{L,i} - \{\mu\}^{n+1,-}_{R,i}\langle\phi\rangle^{n+1,-}_{R,i} + \left(\sigma^{n+1}_{t,i} + \frac{1}{c\Delta t}\right)h_i\langle\phi\rangle^{n+1,-}_{R,i} - \frac{\sigma_{s,i}h_i}{2}\left(\langle\phi\rangle^{n+1,+}_{R,i} + \langle\phi\rangle^{n+1,-}_{R,i}\right) = \frac{h_i}{2}\langle\sigma^{n+1}_a acT^{n+1,4}\rangle_{R,i} + \frac{h_i}{c\Delta t}\langle\phi\rangle^{n,-}_{R,i}, \quad (1.20)$$

Ultimately, the two half-ranges will be treated differently when the equations are closed spatially.

1.1.6 Material Energy Equations

To derive the LO material energy equations, an approximation must be introduced to relate $T(x)$ and $T^4(x)$ within a cell. We represent $T(x)$ spatially with a LDFE trial space. This trial space will ensure preservation of the equilibrium diffusion limit. To simplify the relation between $T(x)$ and $T^4(x)$ $T(x) \simeq T_{L,i}b_{L,i}(x) + T_{R,i}b_{R,i}(x), \quad x \in (x_{i-1/2}, x_{i+1/2})$. Similarly, the emission term is represented in the material and radiation equations with the LDFE interpolant $T^4(x) \simeq T^4_{L,i}b_{L,i}(x) +$

$T^4_{R,i} b_{R,i}(x)$. The L and R spatial moments are taken of the material energy equations; the LDFE representations for $T(x)$ and $\sigma_a acT^4(x)$ are used to simplify the spatial integrals. The final LO material energy equation resulting from application of the L moment is

$$\frac{\rho_i c_{v,i}}{\Delta t}\left[\left(\frac{2}{3}T_{L,i}+\frac{1}{3}T_{R,i}\right)^{n+1}-\left(\frac{2}{3}T_{L,i}+\frac{1}{3}T_{R,i}\right)^{n}\right]+\sigma_{a,i}^{n+1}\left(\langle\phi\rangle^{+}_{L,i}+\langle\phi\rangle^{-}_{L,i}\right)^{n+1} = \sigma_{a,i}^{n+1} ac\left(\frac{2}{3}T^4_{L,i}+\frac{1}{3}T^4_{R,i}\right)^{n+1}. \quad (1.21)$$

The equation for the R moment is

$$\frac{\rho_i c_{v,i}}{\Delta t}\left[\left(\frac{1}{3}T_{L,i}+\frac{2}{3}T_{R,i}\right)^{n+1}-\left(\frac{1}{3}T_{L,i}+\frac{2}{3}T_{R,i}\right)^{n}\right]+\sigma_{a,i}^{n+1}\left(\langle\phi\rangle^{+}_{R,i}+\langle\phi\rangle^{-}_{R,i}\right)^{n+1} = \sigma_{a,i}^{n+1} ac\left(\frac{1}{3}T^4_{L,i}+\frac{2}{3}T^4_{R,i}\right)^{n+1}. \quad (1.22)$$

Cross sections have been assumed constant over each element, evaluated at the average temperature within the element, i.e., $\sigma^{n+1}_{a,i} = \sigma_{a,i}([T^{n+1}_{L,i} + T^{n+1}_{R,i}]/2)$. Because the material energy balance only contains angularly integrated quantities, there is no need to take angular moments of the above equations.

REWRITE: WHAT TO DO WITH THIS PARAGRAPH? Because there are no derivatives of T in Eq. (**??**), there is no need to define T on the faces. Because only moments of ϕ appear in the material energy equations, they are fully defined at this point. The LD closure for the L and $+$ equations produces

1.2 Closing the LO System with Information from the HO Solution

The six degrees of freedom (DOF) over each cell i are the four moments $\langle\phi\rangle^{+}_{L,i}$, $\langle\phi\rangle^{+}_{R,i}$, $\langle\phi\rangle^{-}_{L,i}$, and $\langle\phi\rangle^{-}_{R,i}$ and the two spatial edge values $T_{L,i}$ and $T_{R,i}$. The four

radiation and two material energy equations define a system of equations for the six DOF, coupled spatially through the streaming term. We emphasize that at this point we have not made any spatial or angular approximations to the transport moment equations; these moment equations are exact with respect to the chosen time discretization. The material energy equation has the approximation of an LDFE space for $T(x)$. Some approximation of this form is necessary to relate T and T^4.

1.2.1 Angular Closure

The angular consistency parameters (e.g., Eq. (1.14) and (1.15)) are not known a priori. A lagged estimate of I^{n+1} from the previous HO solve is used to estimate the angular consistency parameters. In the HOLO algorithm, the equations for LO unknowns at iteration $k+1$ use consistency parameters computed using the latest HO solution $\tilde{I}^{n+1,k+1/2}$ as an approximation for $I^{n+1}(x,\mu)$. We evaluate these terms using quadruature based on the functional form of the solution provided by the HO solution.

1.2.2 Spatial Closure

The relation between the volume and face averaged quantities must be known to eliminate the final auxillary unknowns. To close the LO system spatially, we will explore multiple options. The simplest closure is to use a linear-discontinuous (LD) spatial closure with the usual upwinding approximation [13]. For example, for positive flow (e.g., Eq. (**??**)) the face terms $\mu_{i-1/2}$ and $\phi_{i-1/2}$ are upwinded from the previous cell $i-1$ or from a boundary condition; the terms at $x_{i+1/2}$ are linearly extrapolated, computed using the L and R basis moments. By assuming $\phi^{\pm}(x)$ is linear over a cell, a relation between the outflow and moments can be derived, e.g., $\phi^{+}_{i+1/2} = 2\langle\phi\rangle^{+}_{R} - \langle\phi\rangle^{+}_{L}$. For the negative half range, $\phi^{-}_{i-1/2} = 2\langle\phi\rangle^{-}_{L} - \langle\phi_R\rangle^{+}$. The LD

closure, with upwinding, for the L equation and positive half-range is

$$-2\mu_{i-1/2}^{n+1,+}\left(2\langle\phi\rangle_{R,i-1}^{+}-\right)+\{\mu\}_{L,i}^{n+1,+}\langle\phi\rangle_{L,i}^{n+1,+}+\{\mu\}_{R,i}^{n+1,+}\langle\phi\rangle_{R,i}^{n+1,+}+\left(\sigma_{t,i}^{n+1}+\frac{1}{c\Delta t}\right)h_i\langle\phi\rangle_{L,i}^{n+1,+}-\frac{\sigma_{s,i}h_i}{2}\left(\langle\phi\rangle \tag{1.23}$$

Similar equations can be derived for the other directions, fully defining the radiation equations. These equations are equivalent to an S_2

Note that we have chosen to leave $\mu_{i-1/2}^{n+1,+}$ as a value to be estimated from the HO solver, which is more conducive to the other spatial closures described in Sec. **??**. Alternatively, the spatial closure could be introduced before performing the algebraic manipulation to form consistency terms (e.g., into Eq. (1.11)). This would produce only volume-weighted consistency terms for the LD spatial closure.

1.2.2.1 Fixups to LD Solution

The linear-discontinuous (LD) closure with upwinding is not strictly positive. In particular, for optically thick cells with a steep intensity gradient, the solution becomes negative. These negative values of intensity can propagate to adjacent cells. In thick regions of TRT problems, reasonably fine spatial cells can still be on the order of millions of mean free paths; negative values with an LD representation are unavoidable in practice for such cells and mesh refinement is of minimal use. Typically, for a standard LDFE method, the equations are lumped to produce a strictly positive solution (for 1D) [13]. However, standard FE lumping procedures would introduce difficulties in computing the consistency terms from the HO solution. Thus, an alternative spatial closure is used that is equivalent to the standard FE lumping procedure. The L and R moments are defined the same as before, preserving the average within a cell, but the relation between the moments and the outflow is modified. For example, for positive μ, the outflow is now defined as $\phi_{i+1/2}^{+}=\langle\phi\rangle_{R}^{+}$.

Because the basis function $b_{R,i}(x)$ is strictly positive, the outflow is positive. This closure is only used in cells where negative intensities occur.

1.2.3 Newton's Method for LO Equations

Adding the equations for each cell together forms a global system of coupled equations. The equations are nonlinear due to the Planckian emission source. We have used Newton's method to solve the nonlinear system, based on a typical linearization of the Planckian source with cross sections evaluated at temperatures from the previous iteration, as described in [13]. A derivation of the LO Newton equations is given in **??**.

The equations for each half-range are coupled together via scattering. In one spatial dimension, the scattering terms can be included in the discrete system matrix and directly inverted. We consider an alternative iterative solution method that could be more easily extended to higher spatial dimensions in Sec. **??**. Isotropic scattering, including effective scattering terms from the linearization, are included in the system matrix. The system matrix is an asymmetric, banded matrix with a band width of seven and is inverted directly. Newton iterations are repeated until $\phi^{n+1}(x)$ and $T^{n+1}(x)$ are converged to a desired relative tolerance. Convergence is calculated using the spatial L_2 norm of the change in $\phi^{n+1}(x)$ and $T^{n+1}(x)$, relative to the norm of each solution. The lumping-equivalent discretization discussed above is used for cells where the solution for ϕ^{n+1} becomes negative. When negative values for $\phi^{n+1,\pm}(x)$ are detected, the lumping-equivalent discretization is used within those cells and that Newton step is repeated.

1.3 Estimating the Spatial Closure from the HO Solution

REWRITE: Some of this could maybe be moved to the introduction This sections describes an alternative spatial closure to the LO equations based on a parametric relation from the HO solution. In addition to estimating the angular consistency terms, the HO intensity estimates a relation between volume and face-averaged intensities to eliminate the remaining unknowns from the equations. The goal is for the LO moments to reproduce the HO moments more accurately than the LDFE discretization, although additional statistical noise is introduced through face-based tallies. In the remainder of this section, we will motivate the HO spatial closure by forming half range balance equations to form a single unknown for each cell. We will then discuss possible closure relations, based on modifications to standard spatial closures.

1.3.1 Motivation

A half-range balance equation for $\mu > 0$ is formed by adding the exact L and R radation moment equations given by Eq. (1.17) and (1.18), i.e.,

$$\overline{\mu}^{+}_{i+1/2}\phi^{+}_{i+1/2} - \overline{\mu}^{+}_{i-1/2}\phi^{+}_{i-1/2} + \sigma_{a,i}h_i\phi^{+}_{i} = \frac{h_i}{2}q_i, \tag{1.24}$$

where q_i represents the cell-average of all isotropic source terms. In the HOLO method, to reduce the number of unknowns, the angular consistency terms are estimated with the previous HO solution. Additionally, the inflow term $\phi^{+}_{i-1/2}$ is eliminated via upwinding from the previous cell or a boundary condition. An additional equation is needed to eliminate the outflow $\phi^{+}_{i+1/2}$ to produce an equation for a single unknown ϕ^{+}_{i}. Standard spatial discretizations techniques use a fixed approximation for all cells to eliminate the outflow in terms of other unknowns. Alternatively,

the HO solution can be used to estimate a parametric relation between the other uknowns and the outflow, i.e.,

$$\phi^+_{i+1/2} = f(\gamma_i^{HO}, \phi_i^+, \phi^+_{x,i}, \phi^+_{i-1/2}). \tag{1.25}$$

Here, γ_i^{HO} is a constant estimated with the HO solution and f is some function of some number of the input variables. The ECMC solution can provide all of the unknowns in the above equation, so the value of γ_i^{HO} can be determined.

If the problem were linear, or the nonlinear problem was fully converged, then application of this closure can ensure that the HO and LO equations produce the same moments. To produce the same moments, the HO solution must also satisfy the local balance equation, e.g., Eq. (1.24). If any higher moments are introduced through the spatial closure, then the HO solution must also satisfy the same relations as the LO equations. For example, both the LO and HO equation must satisfy the first moment equation in space if the closure is a function of the first moment. then the HO and LO solutions would produce exactly the same moments. There are several issues with ECMC that cause this to not be true, even for a linear problem. With ECMC, global and, particularly, local energy balance are not preserved. There are source biasing techniques for standard MC (e.g., systematic sampling) that exactly preserve the zeroth moment of the source [16, 23]). However, because we have to reconstruct the bilnear moment of x and μ, the consistency terms do not exactly preserve the first moment equation. One final reason is that the analog treatment of absorption (below the weight cutoff, as discussed in Sec. **??**) results in $\sigma_a \phi_i^{HO}$ and the amount of energy removed from a cell during MC transport to not be equal, due to statistical noise in the path-length estimators for ϕ_i^{HO}. However, ECMC will preserve balance to the order of the error, so the closure parameters will reproduce

the HO moments to the accuracy of the LO solution.

REWRITE: THIS IS SAYING WHY LDFE PROJECTION AND LDFE-DISCRETI ZATION ARE NOT EQUAL, PROBALBY JUST DELETE It is noted that the LD projection of the HO solution does not produce the same moments, because MC was used to obtain this projection, the outflow will not agree with the LO equations. For example, the upwinding inflow from a previous cell does not match the actual energy that flowed through that surface due to MC noise.

As TRT problems are non-linear (i.e., scattering or thermal emission are included in q), the moments will only be preserved upon non-linear convergence of the source. The nonlinearity introduces the possibility for stability issues, particularly with MC noise. However, we have already consistently formed angular consistency terms, so the the spatial closure should be more stable than introducing other terms, such as in NDA methods.

REWRITE: MAYBE IT SHOULD GO IN THE INTRO After approximating the angular consistency terms in the time-discretized LO moment equations, there is still more unknowns than equations, for each spatial cell and half range; an extra equation relating the spatial moments and outflow face values is needed, i.e., a spatial closure.

1.3.2 Choice of Spatial Closure

We will explore two different closure relations: a scaled slope, i.e.,

$$\phi^{\pm}_{i\pm1/2} = \phi^{+}_{i} \pm \gamma_i \phi^{+}_{x,i} \tag{1.26}$$

and a scaled average

$$\phi^{\pm}_{i\pm1/2} = \gamma_i \phi^{+}_{i} \pm \phi^{+}_{x,i}, \tag{1.27}$$

where a value of $\gamma_i = 1$ produces the standard linear discontinuous expressions for the extrapolated outflows.

We now use the HO solution to estimate γ_i. For example,

$$\gamma_i^{+,HO} = \frac{\phi_{i+1/2}^+ - \phi_{x,i}^+}{\phi_i^+} \tag{1.28}$$

in the scaled slope case. For this closure, as the slope goes to zero this expression becomes undefined. In cells where the slope is $O(10^{-13}\psi_i)$, we use $\gamma_i = 1$. For the problems tested, no issues have occurred with this closure, even γ can become very large for common, small values of $|\psi^x/\psi_i|$. This is because in such regions the solution is changing minimally anyways. The main benefit of this closure is it allows for values of γ that are equivalent to step ($\gamma_i = 0$) and lumped ($\gamma_i = 1/3$) expressions.

To solve the LO equations, the expression for the outflow face term is substituted in each equation, using the γ_i estimated from the HO solution. There is a spatial closure parameter for each half-range, for each cell. For instance, the positive balance equation becomes

$$\overline{\mu}_{i+1/2}^+ \left(\gamma_i^{+,HO}\phi_i^+ + \phi_{x,i}^+\right) - \overline{\mu}_{i-1/2}^+\phi_{i+1/2}^+ + \frac{\sigma_{a,i}h_i}{2}\phi_i^+ = \frac{h_i}{2}q_i, \tag{1.29}$$

noting that ϕ_i^+ and $\phi_{x,i}^+$ remain as unknowns. The MC solution must be modified to tally the solution on faces. Our LO system is formulated in terms of L and R moments, rather than the average and slope. Thus, the parameteric functions are expressed in terms of the L and R unknowns, using the relations given in App. **??**.

1.3.3 The Doubly-Discontinuous Trial Space

Because of the temperature unknowns and the HO scattering source representation, a representation on the interior of the cell for the temperature and intensity

is needed. However, the outflow from the cell is now a parametric (i.e., non linear) extrapolation of the interior moments. Thus, we introduce a linear doubly discontinuous (LDD) trial space for the half-range intensities, which is depicted in Fig. 1.2. The linear relation on the interior of the cell preserves the L and R moments of the solution. The temperature is still represented with a linear interpolant of T^4 and T. This trial space has an extra unknown outflow, which is eliminated using the HO spatial closure. For the initial LO solve, the outflow is assumed continuous, using the standard upwinding and LD representation. With the outflow term eliminated, the equations have the same numerical complexity as the LD equations.

In the case of strong gradients, the interior representation could be driven negative. Thus, we use the lumped expression to to define the linear representation. For example, the lumped emission source is

$$T = \langle T \rangle_{L,i}^4 b_{L,i}(x) + \langle T \rangle_{R,i}^4 b_{R,i}(x), \quad x \in (x_{i-1/2}, x_{i+1/2}) \tag{1.30}$$

This expression is positive as long as the moments are positive, which is true for physical solutions. If the lagged, MC spatial closure produces an outflow from a cell that is negative, then these moments could become negative. In such cases, we force that cell to use a standard lumped relation for the moment equations, with no discontinuity at the outflow. As verified in Sec. 1.4.1, the interior solution is still second order accurate in space.

During the Newton solve, once new half-range intensities are determined, the temperatures are updated using the moment same moment equations given by Eq. (**??**). This can be confusing because the slope moment, e.g., $\psi_{x,i}^{\pm}$, does not stricly correspond to the slope in the typical since. We have modified it. This is the same as the lumped closure relation using $\gamma_i = 1/3$, where we are preserving the average moment

exactly, but only second order accurate in the slope.

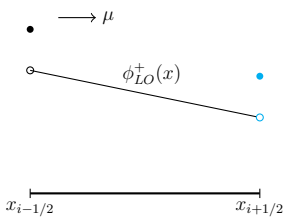

Figure 1.2: Linear doubly-discontinous representation for mean intensity in LO equations

Poor statistics for the face tallies may result in this trial space producing less accurate results compared to the standard LDFE solution, at least for sufficiently fine meshes where LD can accurately represent the solution. Although the closure will be applied everywhere, we expect the greatest improvement in accuracy for cells where the LDFE trial space produces a negative solution.

1.4 Test Problems

To investigate the accuracy and utility of the face closures we compare to the LD spatial closure for two simple test problems. We are interested in the order of convergence on the interior linear solution. We also want to demonstrate a better consistency between the two solvers, particularly at coarser mesh sizes. We also want to compare to the efficiency of LD, noting that the extra noise of the face tallies may make the solution approach not worth it over all.

1.4.1 Order of Convergence

We compute the order of convergence of the linear solution, using a lumped relation for the interior moments. We use the diffusion limit test problem which has

a solution that can be resolved relatively easily with the linear representation and error due to the time discretizaiton will be minimized. fine mesh solution is taken as the reference answer with 800 cells.

REFERENCES

[1] S.R. Bolding and J.E. Morel. A High-Order Low-Order Algorithm with Exponentially-Convergent Monte Carlo for k-Eigenvalue problems. ANS Winter Meeting. Anaheim, CA, 2014.

[2] Jeffery D. Densmore. Asymptotic analysis of the spatial discretization of radiation absorption and re-emission in implicit monte carlo. *Journal of Computational Physics*, 230(4):1116 – 1133, 2011.

[3] Jeffery D Densmore, Kelly G Thompson, and Todd J Urbatsch. A hybrid transport-diffusion monte carlo method for frequency-dependent radiative-transfer simulations. *Journal of Computational Physics*, 231(20):6924–6934, 2012.

[4] J. A. Fleck, Jr. and J. D. Cummings, Jr. An implicit monte carlo scheme for calculating time and frequency dependent nonlinear radiation transport. *J. Comput. Phys.*, 8(3):313–342, December 1971.

[5] N. A. Gentile and Ben C. Yee. Iterative implicit monte carlo. *Journal of Computational and Theoretical Transport*, 0(0):1–31, 0.

[6] N.A. Gentile. Implicit monte carlo diffusion: An acceleration method for monte carlo time-dependent radiative transfer simulations. *Journal of Computational Physics*, 172(2):543–571, 2001.

[7] Eugene D. Brooks III, Michael Scott McKinley, Frank Daffin, and Abraham Szke. Symbolic implicit monte carlo radiation transport in the difference formulation: a piecewise constant discretization. *Journal of Computational Physics*, 205(2):737 – 754, 2005.

[8] Eugene D. Brooks III, Abraham Szke, and Jayson D.L. Peterson. "piecewise linear discretization of symbolic implicit monte carlo radiation transport in the difference formulation ". *"Journal of Computational Physics "*, "220"(1):471 – 497, 2006.

[9] Samet Y Kadioglu, Dana A Knoll, Robert B Lowrie, and Rick M Rauenzahn. A second order self-consistent imex method for radiation hydrodynamics. *Journal of Computational Physics*, 229(22):8313–8332, 2010.

[10] Elmer Eugene Lewis and Warren F Miller. *Computational methods of neutron transport*. John Wiley and Sons, Inc., New York, NY, 1984.

[11] Michael Scott McKinley, Eugene D Brooks III, and Abraham Szoke. Comparison of implicit and symbolic implicit monte carlo line transport with frequency weight vector extension. *Journal of Computational Physics*, 189(1):330–349, 2003.

[12] Dimitri Mihalas and Barbara Weibel-Mihalas. *Foundations of radiation hydrodynamics*. Courier Corporation, 1999.

[13] J.E. Morel, T.A. Wareing, and K. Smith. Linear-Discontinuous Spatial Differencing Scheme for S_n Radiative Transfer Calculations. *Journal of Computational Physics*, 128:445–462, 1996.

[14] H. Park, J.D. Densmore, A.B. Wollaber, D.A. Knoll, and R.M. Ramenzahn. Monte Carlo Solution Methods in a Moment-Based Scale-Bridging Algorithm For Thermal Radiative Transfer Problems. M&C. Sun Valley, ID, 2013.

[15] J.R. Peterson. Exponentially Convergent Monte Carlo for the 1-d Transport Equation. Master's thesis, Texas A&M, 2014.

[16] J.K. Shultis and W.L. Dunn. *Exploring Monte Carlo Methods*. Academic Press, Burlington, MA 01803, 2012.

[17] Clell J Solomon. *Discrete-ordinates cost optimization of weight-dependent variance reduction techniques for Monte Carlo neutral particle transport*. PhD thesis, Kansas State University, 2010.

[18] James M Stone and Michael L Norman. Zeus-2d: A radiation magnetohydrodynamics code for astrophysical flows in two space dimensions. i-the hydrodynamic algorithms and tests. *The Astrophysical Journal Supplement Series*, 80:753–790, 1992.

[19] E.F. Toro. *Riemann Solvers and Numerical Methods for Fluid Dynamics: A Practical Introduction*. Springer, 1999.

[20] J. Willert, C.T. Kelly, D.A. Knoll, and H. Park. A Hybrid Approach to the Neutron Transport k-Eigenvalue Problem using NDA-based Algorithms. M&C. Sun Valley, ID, 2013.

[21] Jeffrey Willert and H. Park. Residual monte carlo high-order solver for moment-based accelerated thermal radiative transfer equations. *Journal of Computational Physics*, 276:405 – 421, 2014.

[22] Allan B Wollaber. *Advanced Monte Carlo methods for thermal radiation transport*. PhD thesis, The University of Michigan, 2008.

[23] Allan B Wollaber. Four decades of implicit monte carlo. *Journal of Computational and Theoretical Transport*, 45(1-2):1–70, 2016.

[24] Allan B Wollaber, Edward W Larsen, and Jeffery D Densmore. A discrete maximum principle for the implicit monte carlo equations. *Nuclear Science and Engineering*, 173(3):259–275, 2013.

[25] Allan B. Wollaber, H. Park, R.B. Lowrie, R.M. Rauenzahn, and M.E. Cleveland. Radiation hydrodynamics with a high-order, low-order method. In *ANS Topical Meeting, International Topical Meeting on Mathematics and Computation*, Nashville Tennessee, 2015.

[26] Ryan T Wollaeger, Allan B Wollaber, Todd J Urbatsch, and Jeffery D Densmore. Implicit monte carlo with a linear discontinuous finite element material solution and piecewise non-constant opacity. *Journal of Computational and Theoretical Transport*, pages 00–00, 2016.

[27] E.R. Wolters. *Hybrid Monte Carlo - Deterministic Neutron Transport Methods Using Nonlinear Functionals*. PhD thesis, Michigan, 2011.